Miner Deposita (2009) 44:705–718
DOI 10.1007/s00126-009-0236-4

ARTICLE

Faulting and fluid flow in porous rocks and sediments: implications for mineralisation and other processes

A. C. Barnicoat · H. A. Sheldon · A. Ord

Received: 5 January 2009 / Accepted: 4 March 2009 / Published online: 7 May 2009

Abstract Faults in sedimentary rocks can act as fluid pathways or barriers to flow and display a range of deformation styles. These features can be explained by behaviours observed in deformation experiments on sedimentary rocks that reveal a transition from dilatant brittle faulting and permeability enhancement to cataclasis and permeability reduction, with increasing porosity, grain size and confining pressure. This transition implies that faults in sedimentary rocks are unlikely to act as fluid pathways shallower than ~3 km, unless the sediments have undergone early cementation, or have been exposed following burial and uplift. This has important implications for many geological processes, including fluid circulation in geothermal systems, formation of sediment-hosted mineral deposits and earthquakes in subduction zones. Stratiform Zn–Pb deposits that have been interpreted as syngenetic, seafloor deposits could instead be interpreted as early epigenetic deposits representing the depth at which faults change from fluid pathways to barriers.

Editorial handling: P. Williams

A. C. Barnicoat (✉)
Predictive Mineral Discovery Co-operative Research Centre,
Geoscience Australia,
GPO Box 378, Canberra, ACT 2601, Australia
e-mail: andrew.barnicoat@ga.gov.au

H. A. Sheldon · A. Ord
Predictive Mineral Discovery Co-operative Research Centre,
CSIRO Exploration and Mining,
P.O. Box 1130, Bentley, WA 6102, Australia

H. A. Sheldon
e-mail: Heather.Sheldon@csiro.au

A. Ord
e-mail: Alison.Ord@csiro.au

Keywords Faulting · Permeability · Fluid flow · Mineralisation

Introduction

Faults are considered in the ore geology community to represent by far the most important fluid flow pathways in hydrothermal systems (e.g. Lindgren 1933; Cox et al. 2001; Sibson 2001). The relevance of permeable faults for hydrothermal mineralisation lies in their ability to focus fluid flow, which is essential for the development of economic concentrations of ore minerals (e.g. Sibson et al. 1988; Cox et al. 2001; Sibson 2001; Zhao et al. 2006). Evidence for fluid flow along faults is recorded by the precipitation of vein material and the development of alteration around faults. In contrast, it is known that faults in hydrocarbon reservoirs and other porous rocks can act either as fluid pathways or as barriers to flow (e.g. Knipe 1992; 1993; Aydin 2000; Fisher and Knipe 2001). Faults may act as barriers to flow by juxtaposing relatively impermeable rock against reservoir rock, by formation of clay smears due to entrainment of clay minerals from the wall rocks or by formation of fault rock with permeability that is lower than that of the host rock. Low permeability fault rocks are formed by cataclasis, compaction, pressure solution and cementation. This type of fault can act as a barrier to flow *within* a hydrocarbon reservoir, resulting in compartmentalisation of fluids and impeding hydrocarbon recovery (e.g. Antonellini and Aydin 1994; Fisher and Knipe 1998).

The reason for the dichotomy of views on fault permeability between the ore geology community and the petroleum geology community lies in the differing mechanical behaviour of rocks that host hydrothermal ore deposits

and those that act as reservoirs for hydrocarbons. For example, orogenic gold deposits are hosted in intensely deformed and metamorphosed rocks (e.g. Groves et al. 1998) with very low porosity, in which faults form by linking and re-activation of discrete fractures (e.g. Scholz 2002; Lockner 1995). Conversely, hydrocarbons typically accumulate in high porosity sedimentary rocks, such as sandstones, in which faulting typically begins with the formation of deformation bands rather than discrete fractures (e.g. Antonellini and Aydin 1994; Fossen et al. 2007). Most research on fault permeability in porous rocks has been driven by the hydrocarbon industry, focussing in particular on faults in sandstones as these are some of the most important reservoir rocks. However, the permeability of faults in porous rocks has relevance beyond the sphere of petroleum geology and reservoir engineering. In this paper, we review some of the literature on fault permeability and deformation mechanisms in porous rocks and consider implications for processes outside the realm of petroleum geology, including fluid circulation in geothermal systems, formation of sediment-hosted mineral deposits and the depth of earthquakes in subduction zones.

Terminology

We define a fault as a tabular region of rock that accommodates shear displacement between the blocks either side of it. A fault may include deformation bands, slip surfaces and fault rock (e.g. cataclasite or fault gouge). Faults represent locations of strain localisation.

We restrict our attention to faults in the upper crust, above the brittle–ductile transition. However, brittle deformation mechanisms can give rise to macroscopically ductile behaviour (Wong et al. 1997; Paterson and Wong 2005). We use the term ‘ductile’ to refer to macroscopic behaviour associated with cataclastic flow. Cataclastic flow in the upper crust is associated with compaction and permeability reduction, whereas ductile deformation in the mid to lower crust tends to be dilatant (Wong et al. 1997; Zhu and Wong 1997). Thus, ductile shear zones in the mid to lower crust may act as fluid pathways, while ductile deformation in the upper crust tends to inhibit fluid flow. Dilatant ductile shear zones are not considered in this paper.

The terms dilation and compaction are used here to describe changes in porosity due to deformation. Dilation and compaction can arise from both elastic (reversible) and inelastic (irreversible) deformation. Reversible deformation of porous rocks is sometimes described as poroelastic behaviour.

Variations in deformation style with porosity are a key focus of this paper. Many processes influence porosity, including gravitational compaction (which may be reversible or irreversible), cementation and generation of secondary porosity by dissolution. We assume that the effect of porosity on deformation is the same regardless of the process(es) that have influenced porosity in a given rock. This is likely to be an oversimplification, but it suffices for the purpose of the present discussion.

Fault zone characteristics

The literature on fault architecture and permeability is voluminous. Here, we present a brief overview in order to emphasise the key features of and differences between faults in low porosity and high porosity rocks.

Faults in low porosity rocks typically comprise a narrow core of fault gouge or cataclasite, which accommodates most of the slip on the fault, surrounded by a wider damage zone containing minor faults, fractures and folds (e.g. Caine et al. 1996). Caine et al. (1996) estimated the permeability of the damage zone in the Dixie Valley fault zone to be two to three orders of magnitude greater than that of the unfractured host rock, while the fault core was estimated to have permeability two to three orders of magnitude smaller than the host rock. These estimates are consistent with laboratory measurements of permeability in samples from the protolith, core and damage zone of a fault zone in granitic rock (Evans et al. 1997) and with numerical simulations of fluid flow through fracture networks (Caine and Forster 1999). More extreme permeability contrasts between the damage zone, core and host rock have been suggested on the basis of large-scale permeability estimates derived from borehole measurements (e.g. Barton et al. 1997). The fault core may have relatively high permeability immediately following a fault slip event; this was illustrated by permeability measurements on samples taken from the Nojima Fault shortly after a major slip event, which indicated fault core permeabilities significantly higher than that of the intact host rock, but still two to three orders of magnitude lower than in the damage zone (Lockner et al. 2000). However, the core tends to become sealed relatively rapidly by compaction, pressure solution and cementation, while the fracture network in the damage zone remains permeable over a longer period of time (Renard et al. 2000; Gratier et al. 2003). The contrast in permeability between damage zone and core results in the fault zone being anisotropic with respect to fluid flow, acting as a conduit for focussed fluid flow in the plane of the fault, but tending to inhibit flow across the fault unless the fault core is very thin or discontinuous (Caine et al. 1996; Lockner et al. 2000).

Faults in porous rocks and sediments typically comprise a zone of sheared deformation bands, sometimes cut or bounded by a discrete slip surface (Aydin 1978; Aydin and

Johnson 1978, 1983; Antonellini and Aydin 1994; Shipton and Cowie 2001; Fossen et al. 2007). Deformation bands are narrow tabular zones of grain re-organisation, formed by a combination of grain fracturing (cataclasis), rotation and sliding. Individual deformation bands accommodate only a few millimetres or centimetres of shear displacement, while discrete slip surfaces can accommodate much larger displacements (Aydin and Johnson 1983; Shipton and Cowie 2001). The formation of slip surfaces has been attributed to a mechanical instability that arises as a consequence of strain hardening associated with the formation of deformation bands (Aydin and Johnson 1983; Shipton and Cowie 2001). Slip surfaces may act as transient fluid pathways (Antonellini and Aydin 1994; Shipton and Cowie 2001), but it may be difficult for fluids to access these pathways due to the low permeability of rocks either side of them. Deformation bands range from minor disaggregation zones, which have similar porosity, permeability and grain size to the host rock and thus have minimal impact on fluid flow, to cataclastic shear bands with permeabilities several orders of magnitude lower than that of the host rock, which act as barriers to fluid flow (Antonellini and Aydin 1994; Fossen et al. 2007; Fisher and Knipe 2001). Cataclasis results in permeability reduction by reducing porosity and grain size and by increasing the surface area of fresh quartz which promotes cementation (Fisher and Knipe 1998). Deformation bands in impure sandstones tend to have lower permeability than those in pure quartz sandstones, due to various effects of clay minerals (Fisher and Knipe 1998, 2001). The capacity of deformation bands to act as barriers to flow is illustrated by faults in oilfields which separate oil-saturated rock from oil-free rock (e.g. Antonellini et al. 1999) and by colour changes across deformation bands in the Aztec Sandstone indicating that these structures acted barriers to fluid flow during diagenesis (Eichhubl et al. 2004).

Faults in poorly lithified sediments are similar to those in high porosity rocks, comprising deformation bands and, in some cases, discrete slip surfaces (Heynekamp et al. 1999; Rawling et al. 2001). Sigda et al. (1999) showed that deformation bands in poorly lithified sediments of the Rio Grande Rift can reduce fault-normal permeability by up to three orders of magnitude relative to the undeformed sediment, even at low displacements. Heynekamp et al. (1999) studied a growth fault in poorly lithified sediments in the Rio Grande rift and noted that the fault is represented by a relatively wide zone of deformation bands where it passes through sand-rich layers and by discrete slip surfaces in clay-rich layers. This change in fault zone thickness was attributed to strain hardening associated with the formation of deformation bands in the sandy layers, contrasting with strain softening associated with alignment of clay minerals along discrete slip surfaces in the clay-rich layers. Thus, deformation is more localised in the clay-rich layers, but spreads out in the sandy layers.

While deformation bands are the most common strain localisation feature in porous rocks and sediments (Fossen et al. 2007), discrete fractures have also been observed in porous sandstones and carbonates, both in the field and in core from hydrocarbon reservoirs. Some authors describe these features as joints or sheared joints, implying that they initiated as mode I cracks with subsequent re-activation in shear (e.g. Flodin and Aydin 2004; Davatzes et al. 2003, 2005; Myers and Aydin 2004). Faults that form by this mechanism comprise a fracture network that is superficially similar to the damage zone of faults in low porosity rocks, with similar consequences for permeability and fluid flow. However, permeability enhancement is likely to be less extreme than in low porosity rocks because the host rock already has relatively high permeability. For example, Jourde et al. (2002) estimated permeability enhancement of just one order of magnitude based on detailed field mapping and numerical simulations of fluid flow through fracture networks in the Aztec Sandstone. Similarly, Micarelli et al. (2006) found that permeability was enhanced only two to three times in the fracture network of a fault in high-porosity carbonate rock.

It is not uncommon to find both deformation bands and fractures/sheared joints within a single outcrop and even within the same fault zone. This phenomenon has been attributed to spatial and temporal variations in the loading regime and porosity. For example, the Rotliegendes reservoir of the North Sea contains cataclastic shear bands associated with early extension, which are overprinted by cemented fractures that formed during basin inversion (Fisher and Knipe 2001). The fractures formed after maximum burial and lithification of the host rock, suggesting a change in deformation mechanism due to porosity reduction. Deformation bands in the Aztec Sandstone, NV have been related to a regional thrusting event and are cross-cut by sheared joint faults associated with a switch to strike-slip tectonics (Eichhubl et al. 2004; Flodin and Aydin 2004; Myers and Aydin 2004). Davatzes et al. (2003) suggested that the switch from deformation bands to joints/fractures that is observed in the Chimney Rock fault array, UT could correspond to the onset of exhumation, but might also be related to a change in rheology due to cementation. Davatzes et al. (2005) described joints and sheared joints in dilatant relays along the Moab fault, which is otherwise characterised by deformation bands. The joints overprint earlier deformation bands, and it was suggested that the switch in deformation mechanism could be related to strain hardening associated with the deformation bands. Furthermore, they noted that the density of deformation bands increases in contractional bends or relays, providing further evidence for the dependence of deformation mechanism on mean stress.

Deformation experiments and constitutive models

In this section, we review results of laboratory deformation experiments on rocks of varying porosity and consider how these results can be used to explain the varying deformation styles displayed by natural fault zones. The small sample size and relatively high strain rates employed in laboratory deformation experiments may result in behaviour that is different from that which occurs naturally in the Earth's crust. Caution is therefore required in drawing analogies between metre- to decimetre-scale structures observed in the field and millimetre- to centimetre-scale features observed in laboratory experiments. Nonetheless, laboratory experiments reveal behaviours that are consistent with field observations, which may help us to understand the controls on deformation mechanisms and fault styles in natural environments.

Triaxial and hydrostatic compression tests on sandstones of varying porosity reveal a transition in failure mode from dilatant brittle faulting, to sheared compaction bands, to distributed shear-enhanced compaction (cataclastic flow) with increasing effective pressure (Zhang et al. 1990; Wong et al. 1997; Zhu and Wong 1997; Cuss et al. 2003; Baud et al. 2006). This transition takes place at higher effective pressure with decreasing porosity and grain size (Wong et al. 1997; Fisher et al. 2003) and has been described as the 'low temperature brittle–ductile transition' (e.g. Rutter and Hadizadeh 1991). Note that the term 'ductile' in this context refers to the macroscopic behaviour; the underlying deformation mechanism (cataclasis) is brittle. Permeability measurements on experimentally deformed samples indicate that cataclasis always results in permeability reduction, whereas dilatant brittle failure results in permeability enhancement if the porosity of the host rock is low (<15%), but destroys permeability if the host rock porosity is high (Zhu and Wong 1997; Wong and Zhu 1999; David et al. 2001). Hence, permeability enhancement is possible only in the dilatant brittle faulting regime and then only if the host rock porosity is low.

The yield stresses for dilatant brittle failure, compaction bands and cataclastic flow map out a capped yield envelope in P, Q space (Fig. 1a; Wong et al. 1997; Cuss et al. 2003; Sheldon et al. 2006), where P is effective pressure and Q is the second invariant of the deviatoric stress (equivalent to differential stress in a standard 'triaxial' test). The yield envelope intersects the P-axis at $P=0$ and $P=P^*$, where P^* is the effective pressure at the onset of irreversible porosity reduction due to cataclasis during hydrostatic (isotropic) loading. Hydrostatic compression tests on sandstones with a range of porosities and grain sizes show that P^* increases with decreasing porosity and grain size (Zhang et al. 1990); in other words, a coarse-grained high porosity rock begins to undergo irreversible compaction at lower effective pressure than a fine-grained low porosity rock. The relationship between porosity, grain size and P^* is approximated by:

$$\log P^* = -1.1 \log(\phi r) + 3.5 \quad (1)$$

where P^* is in megapascal, ϕ is porosity and r is grain radius in micrometre (Fisher et al. 2003). Hence, the size of the yield envelope increases with decreasing porosity and grain size (Fig. 1b).

Similar variations in deformation style with porosity and effective pressure are observed in shales (e.g. Graham et al. 1983; Steiger and Leung 1991) and in porous carbonate rocks (Elliott and Brown 1985; Baud et al. 2000; Vajdova et al. 2004), although the deformation mechanism in carbonates may be different from that in sandstones due to the onset of crystal plasticity at relatively low temperature in carbonates.

Following initial yield, sandstones deforming in the dilatant brittle regime tend to undergo strain softening, while deformation in the transitional or ductile regimes results in strain hardening (Cuss et al. 2003; Baud et al. 2006; Wong et al. 1997; Sheldon et al. 2006). This behaviour is consistent with the aforementioned relationship between porosity and P^* (Eq. 1); that is, dilation (porosity increase) leads to strain softening, represented by a decrease in P^* and corresponding decrease in size of the yield envelope, while compaction (porosity decrease associated with cataclasis) leads to strain hardening, represented by an increase in P^* and expansion of the yield envelope. Such behaviour is encapsulated in the concepts of critical state soil mechanics, a theory which was developed to describe the deformation behaviour of soils, but which can also be applied to porous rocks (e.g. Cuss et al. 2003; Sheldon et al. 2006). Sheldon et al. (2006) used the results of deformation experiments to define a relatively simple critical state constitutive model (based on the Modified Cam Clay model; Roscoe and Burland 1968) for porous sandstones, which can be used to simulate the behaviour of porous sandstones under a range of loading regimes. This constitutive model is characterised by an asymmetric elliptical yield envelope in P, Q space, with the size of the yield envelope being determined by P^* (Eq. 1). The peak of the yield envelope occurs at $P/P^*=\alpha$, where α is ~0.45 in porous sandstones (Fig. 1a; Sheldon et al. 2006; Cuss et al. 2003). The model predicts a transition from localised dilatant brittle failure on the left-hand side of the yield envelope ($P/P^*<\alpha$) to distributed shear-enhanced compaction ('ductile' yield) on the right-hand side of the yield envelope ($P/P^*>\alpha$). These behaviours are associated with strain softening and strain hardening, respectively. Strain hardening inhibits localisation in this constitutive model; hence, it does not predict the formation of sheared compaction bands in the transitional regime. Other authors

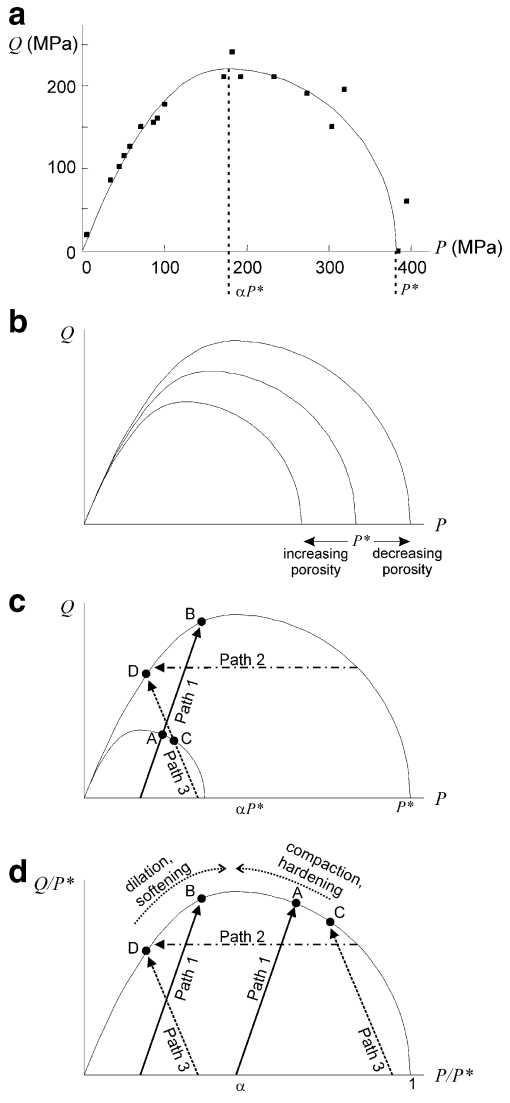

Fig. 1 Yield envelope for porous sandstones. **a** Yield envelope in *P*, *Q* space and yield data for Berea sandstone (Wong et al. 1997). **b** The size of the yield envelope depends on *P**, which decreases with increasing porosity and grain size. Hence, sandstones of different porosity and grain size have yield envelopes of different size and the yield envelope expands/contracts due to changes in porosity during deformation (strain hardening/softening). **c** Effect of different loading paths in *P*, *Q* space. Two yield envelopes represent sandstones of different porosity and/or grain size. *Path 1* represents compression, *Path 2* represents an increase in fluid pressure and *Path 3* represents extension. **d** Same loading paths as in **c** represented in *P*/P**, *Q*/P** space. Points *A*, *B*, *C*, *D* correspond to points in **c**. *Dashed arrows* above yield envelope represent migration of the stress state towards the peak of the yield envelope following initial yield

have proposed more complicated constitutive models which are capable of predicting sheared compaction bands in the transitional regime (e.g. Issen 2002; Ricard and Bercovici 2003; Challa and Issen 2004; Schultz and Siddharthan 2005; Baud et al. 2006). Despite this limitation, the model of Sheldon et al. (2006) predicts a range of behaviours that provide insight into faulting mechanisms of porous rocks.

The predictions of this constitutive model concerning the effects of porosity and loading regime on deformation style are illustrated in Fig. 1c, d. Two yield envelopes are shown in Fig. 1c; the larger envelope corresponds to a rock of lower porosity and/or smaller grain size than the smaller envelope. Fig. 1d shows the yield envelopes normalised to *P**. Three loading paths are shown. Path 1 represents compression (e.g. a typical 'triaxial' compression experiment), with both *P* and *Q* increasing. This loading path reaches the smaller yield envelope in the ductile regime (point A; $P/P^*>\alpha$); the rock would undergo cataclasis and shear-enhanced compaction, resulting in strain hardening and expansion of the yield envelope. The same loading path reaches the larger yield envelope in the dilatant brittle regime (point B; $P/P^*<\alpha$); in this case, the rock would dilate, resulting in strain softening and shrinking of the yield envelope. In both cases, the stress state moves towards the peak of the yield envelope ($P/P^*=\alpha$; Fig. 1d). As the stress state approaches the peak, it takes only a small change in the loading path to move from the ductile regime to the brittle regime, or vice versa. This could explain the observation of deformation bands being overprinted by fractures or sheared joints in dilatant relays along the Moab fault (Davatzes et al 2005) and other cases where a switch from deformation bands to fractures/joints is inferred to correspond to a switch in tectonic regime (Davatzes et al. 2003; Eichhubl et al. 2004; Flodin and Aydin 2004; Myers and Aydin 2004). Strain hardening associated with earlier deformation bands and/or with increasing cementation during burial (e.g. Fisher and Knipe 2001) would facilitate the switch from cataclasis to dilatant brittle faulting.

Path 2 in Fig. 1c, d shows a decrease in *P* at constant *Q*, which could represent the effect of increasing fluid pressure. This is another mechanism which would cause a switch from cataclasis to dilatant brittle faulting.

Path 3 (Fig. 1c, d) represents extensional loading (*P* decreases as *Q* increases). This loading path intersects the smaller yield envelope in the ductile regime (point C) and the larger envelope in the brittle regime (point D). As with path 1, the stress state will move towards the peak of the yield envelope as the rock undergoes strain hardening or strain softening. It is important to note that while the constitutive model can make predictions about the behaviour of rocks undergoing extensional loading, this behaviour has not (to our knowledge) been demonstrated in experiments due to the difficulties with imposing extensional loading paths in the laboratory. However, the predictions of the model seem consistent with field observations; in particular, the observation of a switch from deformation bands to discrete fractures or joints corresponding with a switch from thrust to strike-slip kinematics, or with the onset of exhumation, is consistent with the constitutive model.

Modelling deformation of porous sandstones

Sheldon et al. (2006) incorporated their constitutive model into a finite difference code (FLAC3D; Itasca Consulting Group 2002), which can be used to simulate deformation and fluid flow in porous sandstones under any loading regime. In this code, deformation is coupled with fluid flow through the influence of fluid pressure on effective stress, the effect of dilation/compaction on fluid pressure and the effect of deformation on permeability. Fluid flow is governed by Darcy's law, such that the fluid flux is governed by permeability and by the direction and magnitude of the fluid pressure gradient. Permeability evolves with deformation in accordance with the experimental observations of Zhu and Wong (1997) and David et al. (2001). Full details can be found in Sheldon et al. (2006).

Critical depth for permeability enhancement

We have seen in the previous section that deformation style depends on the value of P/P^* at the point where the loading path intersects the yield envelope. Hence, we might expect a variation in deformation style with depth in a given lithology and given loading regime, because P generally increases with depth and porosity generally decreases with depth (and hence P^* increases, see Eq. 1; Scott and Nielson 1991; Fisher et al. 2003; Sheldon et al. 2006). The rate of porosity reduction with depth depends on the rates of compaction and cementation, which in turn depend on deposition rate, geothermal gradient and grain size (Walderhaug 1996). Figure 2a shows porosity–depth curves for varying grain sizes, geothermal gradients and deposition rates, assuming that porosity reduction is due to temperature-dependent quartz cementation (Walderhaug 1996) combined with mechanical compaction, with no deformation in the horizontal direction (i.e. uniaxial compaction). A high deposition rate, low geothermal gradient and coarse grain size favour preservation of porosity at depth. The corresponding value of P/P^* at first yield, which dictates the deformation style, depends on the loading path that the rock is subjected to following deposition and cementation (c.f. Figs. 1c, d). This is illustrated in Fig. 2b, c, which show P/P^* at first yield for compressional and extensional loading paths, respectively. The compressional loading path results in $P/P^* > \alpha$, implying cataclasis and shear-enhanced compaction, over almost the entire depth range regardless of the deposition rate, grain size and geothermal gradient (Fig. 2b). Conversely, extensional loading results in $P/P^* < \alpha$ over most of the parameter space illustrated in Fig. 2c, which implies dilatant brittle failure according to the model of Sheldon et al. (2006). However, Fisher et al. (2003) note that compaction bands occur from P/P^* as low as 0.25; this means there is a region from ~2 to ~5.5 km depth (depending on parameter values) where dilatant brittle failure gives way to compaction bands in an extensional regime (Fig. 2c).

The variation in porosity and P/P^* with depth is important because it dictates the deformation style and thus determines the depths at which permeability enhancement can occur during deformation. Experimental results suggest that permeability enhancement can occur only in the dilatant brittle faulting regime and then only if the porosity is relatively low (Zhu and Wong 1997). Given the variation in porosity and P/P^* with depth, this implies that there is a critical depth above which permeability enhancement cannot occur, unless the porosity is anomalously low at shallow depths due to early cementation, or due to previous burial followed by uplift and erosion (Scott and Nielson 1991; Fisher et al. 2003; Sheldon et al. 2006). For clean quartz sandstones that have undergone normal burial and cementation, the critical depth for permeability enhancement is estimated to be at least 3.8 km (Fisher et al. 2003; Sheldon et al. 2006). Permeability enhancement may be possible at slightly shallower depths in mudstones, due to earlier cementation associated with release of silica at the smectite–illite transition (Bjørrlykke 1999). Early cementation also occurs in some carbonate depositional settings, but this may be reversed during diagenesis due to dissolution by aggressive fluids that have interacted with organic matter (e.g. Hiatt and Kyser 2000). Hence, the critical depth for permeability enhancement in carbonate sediments will depend on the depositional environment and diagenetic history.

As noted previously, we reiterate the fact that this analysis is based on deformation experiments which followed compressional loading paths. There are no permeability measurements on samples deformed in an extensional regime. The 'sheared joint' faults described by (Eichhubl et al. 2004; Flodin and Aydin 2004; Myers and Aydin 2004; Davatzes et al. 2003, 2005) represent a deformation regime (and possibly a deformation mechanism) that has not been reproduced in experiments; this type of fault might form and result in permeability enhancement, at shallower depths than would be expected based on the preceding analysis.

Variations in deformation style with depth

Figure 3 shows the pattern of volumetric strain (dilation) due to extensional deformation in two scenarios with different initial porosity–depth distributions. The initial size of the model was 12 km wide and 6 km deep. The top of the model was subject to normal stress representing overlying water, the base of the model was fixed in the z

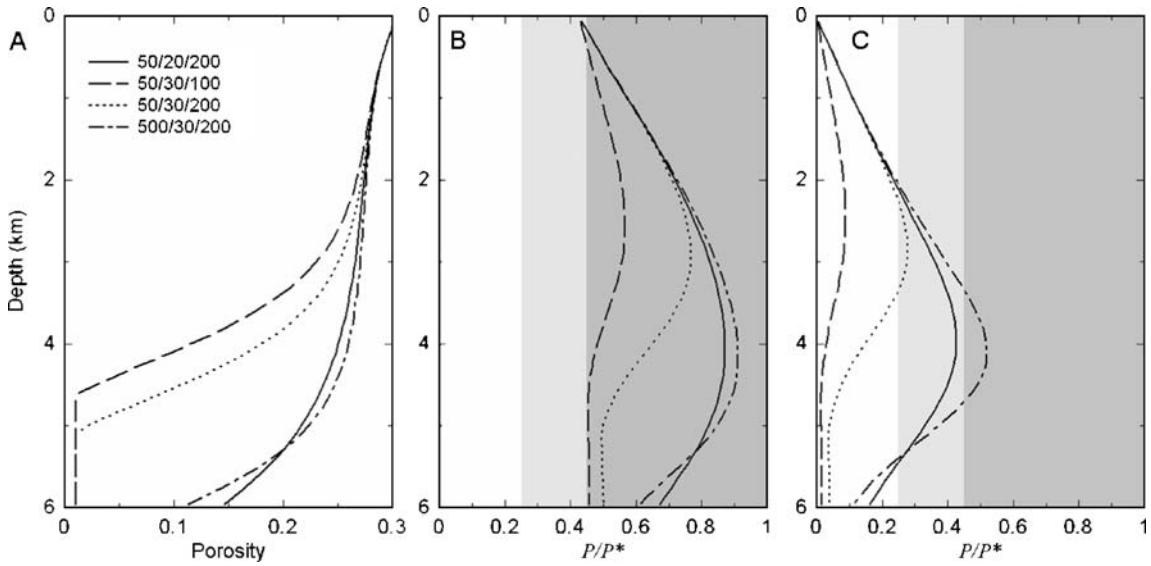

Fig. 2 **a** Porosity versus depth (before deformation). Legend indicates deposition rate (m/Myr)/geothermal gradient (°C/km)/grain diameter (μm). **b** P/P^* at initial yield on a compressional loading path. **c** P/P^* at initial yield on an extensional loading path. *Light and dark shaded areas* in **b** and **c** indicate the brittle–ductile transitional regime ($0.25 \leq P/P^* \leq \alpha$), where compaction bands are expected to form and the distributed shear-enhanced compaction regime ($P/P^* > \alpha$), respectively

(vertical) direction and the ends of the model were moved outwards (x-direction) at constant velocity to simulate extension. There was no movement in the out-of-plane (y) direction. Models a and b underwent spontaneous localisation due to strain softening in the brittle regime, creating pairs of conjugate 'faults'. However, model b has a region from ~4 to 5 km depth where $P/P^* > \alpha$, resulting in distributed cataclasis rather than localised dilatant shear failure. This results in a band of negative volume strain (compaction) across the central part of the model, with the deformation here being less strongly localised than in the brittle layers above and below. This region would be characterised by faults composed of multiple deformation bands in naturally deformed rocks. We reiterate the fact that the constitutive model of Sheldon et al. (2006) cannot predict strain localisation in the ductile regime and so does not predict the formation of narrow faults in this regime. Nonetheless, it captures the change in porosity–permeability evolution of faults with depth, which is the main focus of this paper.

Figure 4 shows permeability normalised to initial permeability in models a and b, with dark grey indicating permeability enhancement and light grey indicating permeability reduction. Permeability enhancement occurs only in the lower portion of model a; this is the only place where porosity is low enough to allow permeability enhancement, even in the dilatant brittle regime. Figure 5 shows the effect of permeability evolution on fluid flow in model a. An initially uniform upward fluid flow field is focussed through the permeable fault zone near the base of the model and then diverges out of the fault zone where it becomes less permeable than the host rocks. Possible implications of this flow pattern are discussed further below.

Deformation in layered sandstones

Figure 6 illustrates the effects of local variations in porosity and grain size between adjacent sedimentary layers. The model comprised three layers, each layer initially 1 km long

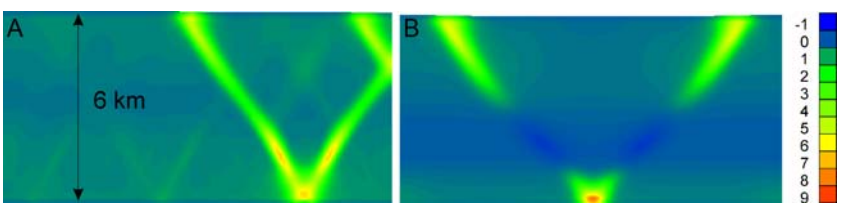

Fig. 3 Percentage volumetric strain (positive = dilation) after 1.5% extension (plane strain). Geothermal gradient 30°C/km, grain diameter 200 μm. Deposition rate=50 (**a**) and 500 m/Ma (**b**); see Fig. 2 for initial porosity–depth curves and P/P^*

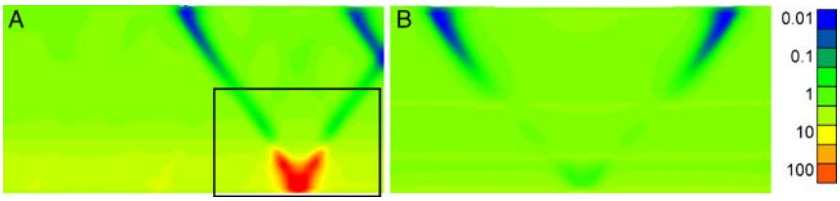

Fig. 4 Permeability normalised to initial permeability in model **a** and **b** after 1.5% extension (plane strain). High values (*dark*) indicate permeability enhancement; low values (*light*) indicate permeability reduction. *Box* in **a** indicates area shown in Fig. 5

and 100 m deep (Fig. 6a). The middle layer had finer grain size and lower porosity than the outer layers. The top of the model was subject to normal stress representing 3 km of overburden. Fluid pressure was initialised at 1.5 times hydrostatic and was fixed at the top and base of the model, generating a uniform upward flow field as the initial condition. The model was shortened in the *x*-direction (plane strain), with the lower boundary fixed in the *z*-direction. This deformation regime resulted in localised dilatant shear failure (Fig. 6b) and permeability enhancement in the middle layer ($P/P^* < \alpha$), while the outer layers underwent distributed shear-enhanced compaction and permeability reduction ($P/P^* > \alpha$). Fluid flow became focussed through the permeable 'fault' in the middle layer (Fig. 6c). The location of the 'fault' close to one end of the model is a numerical artefact and is not significant; in reality, the location of faults would be influenced by pre-existing heterogeneities in the rock mass.

This model shows how lithological variations can dictate whether rocks deform by dilation or compaction under identical conditions. Localised deformation within the finer lower porosity layer acts to focus fluids, whereas broad deformation zones within the higher porosity layers tend to disperse fluid flow. This has implications for the genesis of sediment-hosted mineral deposits, which are discussed further below.

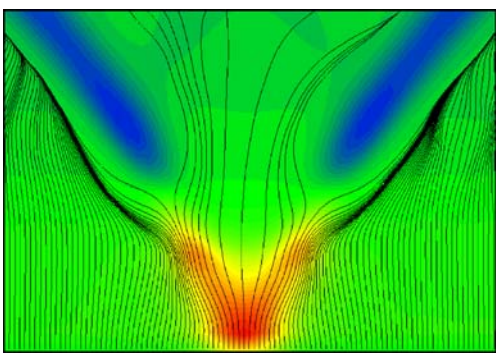

Fig. 5 Fluid flow streamlines (*white*) superimposed on permeability ratio. Area corresponds to *box* in Fig. 4a. Uniform upward flow from the base of the model is focussed into the high permeability part of the fault zones (*dark grey*), then diverges out of the fault zones where they become low permeability barriers (*light grey*)

Discussion

Near-surface sediments

Observations from young (Tertiary–Recent) sediments are consistent with the nature of fluid flow inferred for unlithified or poorly lithified sediments from the concepts discussed above and in Sheldon et al. (2006). In general, fluid flow in these sediments is not controlled by faults but

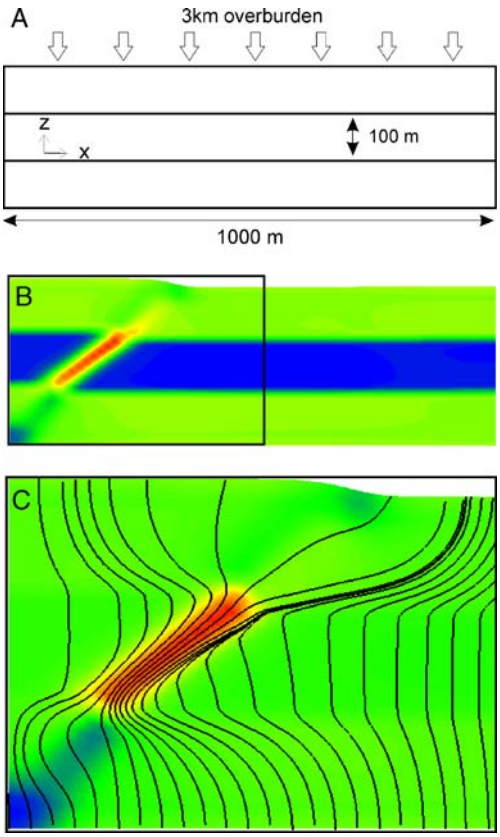

Fig. 6 Layered model. **a** Geometry. Middle layer has finer grain size (radius=100 μm) and lower porosity (0.05) than outer layers (200 μm and 0.1). **b** Porosity after 5.6% shortening. Maximum (*dark grey*)= 0.135, minimum (*white*) = 0.034. Note localised dilation in the mid layer. **c** Permeability ratio (k/k_0) and fluid flow streamlines after 5.6% shortening (enlarged area corresponds to *box* in Fig. 6b). Maximum permeability ratio (*dark grey*)=5.6×10^{1}, minimum (*white*)=4.3×10^{-3}. Fluid flow is focussed through the permeable 'fault' in the mid layer

is either by direct upward migration through porous sediment, or laterally when captured by 'thief' layers. Figure 7 shows an example of vertical gas escape from a reservoir off the south coast of Australia. Note that the gas migrates straight up, rather than along the faults, in a manner consistent with the rock behaviour explored in this paper. An example of similar processes operating in the North Sea is described by Løseth et al. (2003): They show that gas escapes along faults from Jurassic reservoir rocks, until it reaches poorly lithified Tertiary sediments where the gas rises along chimneys that are not related to faults, ultimately leading to the development of 'chaotic zones' high in the stratigraphy. At even shallower levels, pockmarks on the seafloor develop above chimneys that mark the pathways of gas escape (Gay et al. 2003). Typically, arrays of pockmarks develop above buried channel sands that guide the escape of the gas. Similar features have been observed at accretionary wedges (e.g. Henry et al. 2002; Kobayashi 2002).

Earthquake distribution

Observations on the coseismic slip distribution in great subduction zone earthquakes and smaller earthquakes reveal that in environments with young sediments at the surface, tremors do not occur within 5–8 km of the Earth's surface (e.g. Byrne et al. 1988; Marone and Scholz 1988; Moore and Saffer 2001; Fuis et al. 2003, Kao et al. 2005). A range of mechanisms have been suggested to explain this (largely aimed at explaining the distribution of earthquakes in subduction zones), including the thermally induced transformation of smectite to illite which has been inferred to cause a change in mechanical behaviour, changes in fluid production and pressure and increased consolidation with depth (e.g. Hyndman and Wang 1995; Moore and Saffer 2001). Experimental data, however, strongly suggests that the smectite to illite transformation does not lead to an appropriate switch in behaviour (Saffer and Marone 2003). Our hypothesis has been parameterised for clastic sediments somewhat different in composition to the material entering subduction zones. However, the simulated transition from macroscopically ductile compactional behaviours at shallow levels to brittle dilatant behaviours at depth, caused by a decrease in porosity due to compaction coupled with a strengthening and further porosity reduction due to cementation, does appear to be consistent with the changes in mechanical properties inferred from the earthquake studies. As noted by Scholz (2002), changes in bulk rock rheology are typically associated with transitions from stable to unstable (velocity weakening, i.e. earthquake) behaviour. It is thus possible that subducted sediment behaves in a manner similar to the sandstones evaluated by Sheldon et al. (2006).

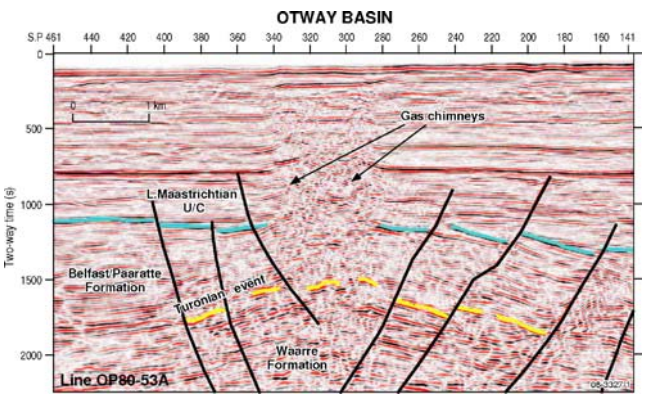

Fig. 7 Gas chimneys developed in upper Cretaceous and younger sediments in the Otway Basin of Victoria, Australia (Cowley and O'Brien 2000). Note how gas escape is not along the faults but vertically upwards through the sediments. This is consistent with the behaviour of porous sediments described in this paper and elsewhere, in that faults in high-porosity sediments are expected to have lower permeability than that of the surrounding undeformed sediments and hence would not act as conduits for fluid flow

Geothermal activity in the Taupo rift zone

In an investigation of hydrothermal processes operating in the Taupo rift zone (New Zealand), Rowland and Sibson (2004) described how thermal convection occurs to a depth of 7–8 km in Mesozoic basement rocks overlain by Quaternary pyroclast-filled basins. Within the basement, flow is focussed through faults and fractures likely to be active in the current stress field. Within the basins, however, faults act as barriers to hydrothermal circulation, creating a series of fluid flow compartments. Such behaviour is consistent with the hypothesis of Sheldon et al. (2006) that the distribution of fluid flow will be strongly influenced by the change in permeability contrast between faults and their host rocks with depth of burial.

Ore deposits

Sediment hosted Zn–Pb systems

The observation of a common association between sediment-hosted Zn–Pb deposits and faults is consistent with our opening remarks that focussed fluid flow, generally associated with structurally derived permeability is a key ingredient in the formation of hydrothermal ore deposits. Some styles of sediment-hosted base metal mineralisation are recognised as epigenetic (e.g. at Lisheen in Ireland; Wilkinson et al. 2005), and their association with faulting is consistent with the model discussed here; that is, the structure hosting the mineralisation formed after sufficient compaction and diagenesis had occurred to

permit deformation in the dilatant brittle regime, thus creating a permeable structure capable of focussing fluid flow. Base metal mineralisation at Mt Isa, Hilton and George Fisher in Queensland (see summaries in Solomon and Groves 1994 and Chapman 2004) is hosted by the Urquhart Shale, a siltstone package that forms part of the Isa Superbasin (Southgate et al. 2000). Much of the ore is in veins and breccias, suggesting that fluid was focussed by dilatant structures formed in rocks that were relatively brittle at the time of deformation, due to diagenesis and compaction during burial. This is confirmed by recent work of Chapman (2004), who inferred that even the earliest bedding–parallel ore formation occurred in rocks that were at least 'semi-consolidated'.

Other examples of Zn–Pb mineralisation associated with faults (such as McArthur River in Queensland, Australia; Large et al. 1998) are stratabound or stratiform and have been interpreted by some workers as syngenetic sedimentary exhalative (SEDEX) deposits resulting from exhalation of ore-forming fluids into euxinic marine environments (Fig. 8a). The McArthur River deposit is hosted in shales, some of which are dolomitic, overlying a thick sequence of dolomites. As noted earlier, the mechanical behaviour of carbonate sediments at high crustal levels is highly variable due to variations in the timing of cementation, but the balance of evidence suggests that deformation of the sediments at McArthur River was more likely to have resulted in permeability reduction than permeability enhancement. In particular, observations of the relationship between early structures and mineralisation by Hinman (1995), who described the deformation as 'ductile', and by Perkins and Bell (1998) reveal that none of the early structures (with the exception of those affecting concretions) were dilatant and that mineral growth in them is absent. Thus, it seems unlikely that fluids would have been focussed in permeable faults all the way to the sea floor, as has been assumed in some numerical modelling studies of SEDEX style ores (Garven et al. 2001; Simms and Garven 2004; Yang et al. 2004). A more realistic modelling approach was taken by Oliver et al. (2006), who assumed that permeable basement faults did not penetrate sedimentary cover in their models of fluid flow across a faulted basement–sediment interface. Their model was not sufficiently detailed to resolve the pattern of fluid flow within the sediments, although it suggested a continuation of focussed upward flow from the basement faults into the overlying sediments.

An alternative explanation for syngenetic or early epigenetic stratiform deposits could be that they form at the depth where a fault changes (upwards) from being a fluid pathway to a fluid barrier (Fig. 8b). Our conceptual model suggests that fluids will not flow along the fault itself at this point: Depending on the permeability

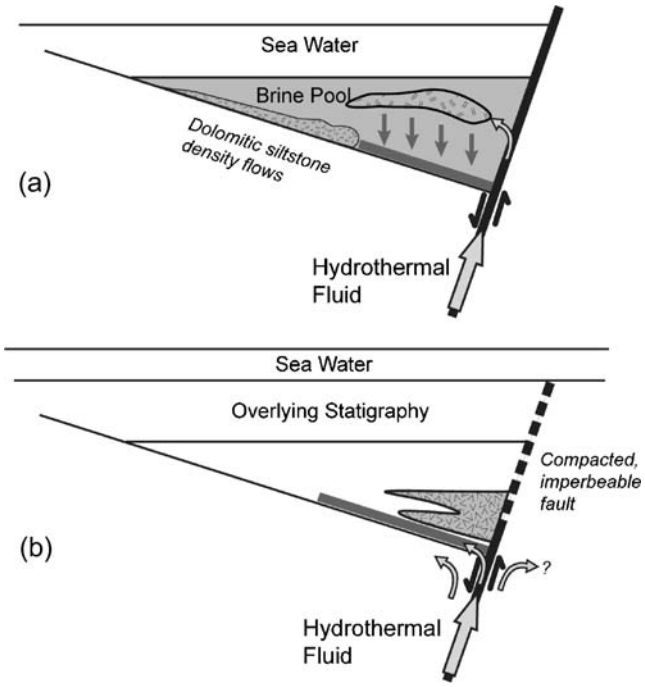

Fig. 8 Conceptual models for the formation of Zn–Pb deposits such as McArthur River and Century in northern Australia. **a** Fluid flow along faults feeding brine pools. Deposition of Zn and Pb sulphides is a response to reaction of upwelling metal-bearing fluid with sulphide generated in the brine pool or the underlying sediment (after Large et al. 1998, 2001). **b** Fluid migration up fault until it reaches the level at which the fault rock becomes less permeable than the host rocks. At this level, fluid migrates laterally and ore formation occurs by fluid-rock reaction and/or fluid mixing. Model **a** assumes that the fault acts as a fluid conduit all the way to the sea floor, which is unlikely unless the sediments have been uplifted or cemented at very shallow depths. Model **b** is consistent with the behaviour of porous sediments discussed in this paper

of the host rocks and the hydrological regime, the fluid may continue to rise upwards adjacent to the fault (e.g. Fig. 5) or may disperse into the sediments. This mechanism is consistent with the behaviours described for hydrothermal systems at sediment-covered spreading centres by Goodfellow and Zierenberg (1999) and with the view of the 'diapiric upwelling of hydrothermal fluid' envisaged by McKibben et al. (1988) in the Salton Sea geothermal system and by Lydon et al. (2000) in the Proterozoic Zn–Pb hydrothermal system at Sullivan in British Columbia.

Unconformity uranium deposits

Uranium mineralisation occurs above, at and below the basal unconformity of Proterozoic sedimentary basins in Canada and Australia (Ruzicka 1996; Mernagh et al. 1998), and a spatial association of these uranium ore bodies with basement-penetrating faults is well established. Detailed observations are sparse, but it is clear that re-activation of

basement structures post-dated the deposition of sandstones and was associated with alteration and mineralisation. Kotzer and Kyser (1995) describe alteration and anomalous geochemistry associated with reverse-re-activated basement faults cutting the overlying sandstones, and Beaufort et al. (2005) report very similar relationships in the Alligator Rivers area of northern Australia. Although the descriptions of quartz and sudoite textures presented by Kotzer and Kyser (1995) are suggestive of alteration as a response to flow along a dilatant fault, it is not possible to distinguish between this and fluids flowing adjacent to the fault in the case that it acted as a barrier to flow (see Sibson 2000; Fig. 7). However, Tourigny et al. (2001) showed that re-activated reverse faults host ore in the basement and are associated with brecciation and fracturing in the overlying Athabasca Sandstone. Similarly, Beaufort et al. (2005) in their description of alteration in the Kombolgie sandstones in northern Australia noted that mineralisation-related alteration occurs in fractures within fault zones and that rocks affected by early alteration are themselves brecciated and re-cemented by later alteration. These observations clearly show that dilatant brittle deformation occurred in these systems, implying sufficient depth of burial in order for the sandstones to have reached a porosity low enough for such brittle deformation to prevail. The exact depth is difficult to determine as it depends on many factors including grain size and geothermal gradient, but it is likely to have been at least 3–4 km based on the models of Sheldon et al. (2006). This depth estimate based on our analysis of changing deformation style with burial and diagenesis is entirely compatible with the independent depth estimates of 5–7 km for the Athabasca systems (Pagel et al. 1980) and >4 km for the Australian Kombolgie sandstone (Derome et al. 2003). It should be noted, however, that Hiatt et al. (2001) suggested that cementation in these basins may have commenced at unusually shallow levels (<1 km), which would raise the depth at which dilatant faulting and permeability enhancement could have occurred.

Summary

Faults in sedimentary rocks display a range of deformation styles, including deformation bands, discrete slip surfaces and sheared fractures/joints. Faults that are dominated by deformation bands tend to act as barriers to fluid flow, while those characterised by discrete fractures act as fluid pathways.

The characteristics of natural faults in sedimentary rocks can be explained by behaviours observed in deformation experiments. Such experiments suggest that sandstones and other porous rocks undergo a transition from dilatant brittle faulting to macroscopically ductile behaviour (including formation of compaction bands) with increasing porosity, grain size and confining pressure. The implication of this 'brittle-ductile' transition is that faults in sedimentary rocks are unlikely to act as fluid pathways at depths shallower than ~3 km, unless the sediments have undergone unusually early cementation, or have been exposed following burial and uplift. Fluid that is focussed through permeable faults at depth may continue to be guided by the fault at shallow depths, but will migrate through the sediments adjacent to the fault rather than through the fault itself. Alternatively, fluids may become dispersed away from the fault through the stratigraphy, depending on the hydrology and permeability distribution.

We have discussed the implications of this behaviour for gas migration through young sediments, the distribution of earthquakes in subduction zones, the pattern of fluid flow in the Taupo rift zone and the formation of sediment-hosted ore deposits. These examples serve to illustrate the importance of understanding the mechanisms of faulting in sedimentary rocks and the consequences for permeability, in order to understand the effect of faults on fluid flow. In particular, we wish to emphasise that faults in porous sedimentary rocks do not necessarily act as fluid pathways; this should be taken into account in models of hydrothermal systems.

Acknowledgements We are grateful to Rick Sibson and Peter Southgate for discussions and suggestions and to Quentin Fisher for a preprint of a manuscript in press. Roger Skirrow and Paul Henson reviewed an earlier version of the manuscript and helped to clarify a number of issues. Nick Oliver, an anonymous referee, and editor Pat Williams are thanked for helpful comments on the manuscript. The work reported here was conducted as part of the Predictive Mineral Discovery Cooperative Research Centre (pmd*CRC) and is published with the permission of the CEOs of the pmd*CRC and Geoscience Australia.

References

Antonellini M, Aydin A (1994) Effect of faulting on fluid flow in porous sandstones: petrophysical properties. Am Assoc Pet Geol Bull 78:355–377

Antonellini M, Aydin A, Orr L (1999) Outcrop-aided characterization of a faulted hydrocarbon reservoir: Arroyo Grande Oil Field, California, USA. In: Haneberg WC, Mozley P, Moore JC, Goodwin LB (eds) Faults and subsurface fluid flow in the shallow crust: Geophys Monogr 113. American Geophysical Union, Washington, pp 7–26

Aydin A (1978) Small faults formed as deformation bands in sandstone. Pure Appl Geophys 116:913–930

Aydin A (2000) Fractures, faults, and hydrocarbon entrapment, migration and flow. Mar Pet Geol 17:797–814

Aydin A, Johnson AM (1978) Development of faults as zones of deformation bands and as slip surfaces in sandstone. Pure Appl Geophys 116:931–942

Aydin A, Johnson AM (1983) Analysis of faulting in porous sandstones. J Struct Geol 5:19–31

Barton CA, Hickman S, Morin R, Zoback MD, Finkbeiner T, Sass J, Benoit D (1997) Fracture permeability and its relationship to in-situ stress in the Dixie Valley, Nevada, geothermal reservoir. Proceedings of the 22nd Workshop on Geothermal Reservoir Engineering, SGP-TR-156, Stanford University, California

Baud P, Schubnel A, Wong TF (2000) Dilatancy, compaction, and failure mode in Solnhofen limestone. J Geophys Res 105:19289–19303

Baud P, Vajdova V, Wong TF (2006) Shear-enhanced compaction and strain localization: inelastic deformation and constitutive modeling of four porous sandstones. J Geophys Res 111:B12401. doi:10.1029/2005JB004101

Beaufort D, Patrier P, Laverret E, Bruneton P, Mondy J (2005) Clay alteration associated with Proterozoic unconformity-type uranium deposits in the east Alligator Rivers uranium field, Northern Territory, Australia. Econ Geol 100:515–536

Bjørrlykke K (1999) Principal aspects of compaction and fluid flow in mudstones. Geol Soc Lond Spec Pub 158. Geological Society of London, London, pp 73–78

Byrne DE, Davis DE, Sykes LR (1988) Loci and maximum size of thrust earthquakes and the mechanism of the shallow region and subduction zone earthquakes. Tectonics 7:833–857

Caine JS, Forster CB (1999) Fault zone architecture and fluid flow: Insights from field data and numerical modelling. In: Haneberg WC, Mozley PS, Moore JC, Goodwin LB (eds) Faults and subsurface fluid flow in the shallow crust: Geophys Monogr 113. American Geophysical Union, Washington, pp 101–127

Caine JS, Evans JP, Forster CB (1996) Fault zone architecture and permeability structure. Geology 24:1025–1028

Challa V, Issen KA (2004) Conditions for compaction band formation in porous rock using a two-yield surface model. J Eng Mech ASCE 130:1089–1097

Chapman LH (2004) Geology and mineralization styles of the George Fisher Zn–Pb–Ag deposit, Mount Isa, Australia. Econ Geol 99:233–255

Cowley R, O'Brien GW (2000) Identification and interpretation of leaking hydrocarbons using seismic data; a comparative montage of examples from the major fields in Australia's North West Shelf and Gippsland Basin. Aust Pet Prod Explor Assoc J 40: 121-150

Cox SF, Knackstedt MA, Braun J (2001) Principles of structural control on permeability and fluid flow in hydrothermal systems. Rev Econ Geol 14:1–24

Cuss RJ, Rutter EH, Holloway RF (2003) The application of critical state soil mechanics to the mechanical behaviour of porous sandstones. Int J Rock Mech Min Sci 40:847–862

Davatzes NC, Aydin A, Eichhubl P (2003) Overprinting faulting mechanisms during the development of multiple fault sets in sandstone, Chimney Rock fault array, Utah, USA. Tectonophysics 363:1–18

Davatzes NC, Eichhubl P, Aydin A (2005) Structural evolution of fault zones in sandstone by multiple deformation mechanisms: Moab fault, Southeast Utah. Geol Soc Am Bull 117:135–148

David C, Menendez B, Zhu W, Wong TF (2001) Mechanical compaction, microstructures and permeability evolution in sandstones. Phys Chem Earth 26:45–51

Derome D, Cuney M, Cathelineau M, Fabre C, Dubessy J, Bruneton P, Hubert A (2003) A detailed fluid inclusion study in silicified breccias from the Kombolgie sandstones (Northern Territory, Australia): inferences for the genesis of middle-Proterozoic unconformity-type uranium deposits. J Geochem Explor 80:259–275

Eichhubl P, Taylor WL, Pollard DD, Aydin A (2004) Paleo-fluid flow and deformation in the aztec sandstone at the Valley of Fire, Nevada—evidence for the coupling of hydrogeologic, diagenetic, and tectonic processes. Geol Soc Am Bull 116:1120–1136

Elliott GM, Brown ET (1985) Yield of a soft, high porosity rock. Geotechnique 35:413–422

Evans JP, Forster CB, Goddard JV (1997) Permeability of fault-related rocks, and implications for hydraulic structure of fault zones. J Struct Geol 19:1393–1404

Fisher QJ, Knipe RJ (1998) Fault sealing processes in siliciclastic sediments. In: Jones G, Fisher QJ, Knipe RJ (eds) Faulting, fault sealing and fluid flow in hydrocarbon reservoirs: Geol Soc Lond Spec Pub 147. Geological Society of London, London, pp 117–134

Fisher QJ, Knipe RJ (2001) The permeability of faults within siliciclastic petroleum reservoirs of the North Sea and Norwegian continental shelf. Mar Pet Geol 18:1063–1081

Fisher QJ, Casey M, Harris SD, Knipe RJ (2003) Fluid-flow properties of faults in sandstone: the importance of temperature history. Geology 31:965–968

Flodin EA, Aydin A (2004) Evolution of a strike-slip fault network, Valley of Fire state park, Southern Nevada. Geol Soc Am Bull 116:42–59

Fossen H, Schultz RA, Shipton ZK, Mair K (2007) Deformation bands in sandstone: a review. J Geol Soc 164:755–769

Fuis GS, Clayton RW, Davis PM, Ryberg T, Lutter WJ, Okaya DA, Hauksson E, Prodehl C, Murphy JM, Benthien M, Baher SA, Kohler MD, Thygesen K, Simila G, Keller GR (2003) Fault systems of the 1971 San Fernando and 1994 Northridge earthquakes, southern California: relocated aftershocks and seismic images from LARSE II. Geology 31:171–174

Garven G, Bull SW, Large RR (2001) Hydrothermal fluid flow models of stratiform ore genesis in the McArthur Basin, Northern Territory, Australia. Geofluids 1:289–311

Gay A, Lopez M, Cochant P, Sultan N, Cauquil E, Brigaud F (2003) Sinuous pockmark belt as indicator of shallow buried turbiditic channel on the lower slope of the Congo basin, West African margin. Geol Soc Lond Spec Pub 216. Geological Society of London, London, pp 173–189

Goodfellow WD, Zierenberg RA (1999) Genesis of massive sulphide deposits at sediment-covered spreading centers. Rev Econ Geol 8:297–324

Graham J, Noonan ML, Lew KV (1983) Yield states and stress–strain relationships in a natural plastic clay. Can Geotech J 20:502–516

Gratier JP, Favreau P, Renard F (2003) Modeling fluid rransfer along California faults when integrating pressure solution crack sealing and compaction processes. J Geophys Res 108:2104–2129

Groves DI, Goldfarb RJ, Gebre-Mariam M, Hagemann SG, Robert F (1998) Orogenic gold deposits: a proposed classification in the context of their crustal distribution and relationship to other gold deposit types. Ore Geol Rev 13:7–27

Henry P, Lallelmant S, Nakamura K, Tsunogai U, Mazzoti S, Kobayashi K (2002) Surface expression of fluid venting at the toe of the Nankai wedge and implications for flow paths. Mar Geol 187:149–183

Heynekamp MR, Goodwin LB, Mozley PS, Haneberg WC (1999) Controls on fault-zone architecture in poorly lithified sediments, Rio Grande Rift, New Mexico: implications for fault-zone permeability and fluid flow. In: Haneberg WC, Mozley P, Moore JC, Goodwin LB (eds) Faults and subsurface fluid flow in the shallow crust: Geophys Monogr 113. American Geophysical Union, Washington, pp 27–50

Hiatt EE, Kyser K (2000) Links between depositional and diagenetic processes in basin analysis: porosity and permeability evolution in sedimentary rocks. Min Assoc Can Short Course Ser 28:63–92

Hiatt EE, Fayek M, Kyser K, Polito P (2001) The importance of early quartz cementation events in the evolution of aquifer properties of ancient sandstones: isotopic evidence from ion probe analysis of sandstones from the McArthur, Athabasca, and Thelon basins. Geol Soc Am Abstr Progr 33:A74

Hinman M (1995) Base metal mineralisation at McArthur River: structure and kinematics of the HYC-Cooley zone at McArthur River. Aust Geol Surv Organ Rec 1995/5, Aust Geol Surv Organ, Canberra

Hyndman RD, Wang K (1995) Thermal constraints on the seismogenic portion of the southwestern Japan subduction thrust. J Geophys Res 100:15373–15392

Issen KA (2002) The influence of constitutive models on localization conditions for porous rock. Eng Fract Mech 69:1891–1906

Itasca Consulting Group (2002) FLAC3D: fast lagrangian analysis of continua in 3 dimensions. Itasca, Minneapolis, MN

Jourde H, Flodin EA, Aydin A, Durlofsky LJ, Wen XH (2002) Computing permeability of fault zones in eolian sandstone from outcrop measurements. Am Assoc Pet Geol Bull 86:1187–1200

Kao H, Shan S-J, Dragert H, Rogers G, Cassidy JF, Ramachandran K (2005) A wide depth distribution of seismic tremors along the northern Cascadia margin. Nature 436:841–844

Knipe RJ (1992) Faulting processes and fault seal. In: Larsen RM, Brekke H, Larsen BY, Talleraas E (eds) Nor Pet Soc Spec Pub 1. Elsevier, New York, pp 325–342

Knipe RJ (1993) The influence of fault zone processes and diagenesis on fluid flow. In: Horbury AD, Robinson AG (eds) Diagenesis and basin development: Am Assoc Pet Geol Stud Geol 36. American Association of Petroleum Geologists, Tulsa, pp 135–154

Kobayashi K (2002) Tectonic significance of the cold seepage zones in the eastern Nankai accretionary wedge—an outcome of the 15 years' KAIKO projects. Mar Geol 187:3–30

Kotzer TG, Kyser TK (1995) Petrogenesis of the Proterozoic Athabasca basin, northern Saskatchewan, Canada, and its relation to diagenesis, hydrothermal uranium mineralization and paleohydrology. Chem Geol 120:45–89

Large R, Bull SW, Cooke DR, McGoldrick PJ (1998) A genetic model for the HYC deposit, Australia: based on regional sedimentology, geochemistry, and sulphide–sediment relationships. Econ Geol 93:1345–1368

Lindgren W (1933) Mineral deposits. McGraw Hill, New York

Lockner D, Naka H, Tanaka H, Ito H, Ikeda R (2000) Permeability and strength of core samples from the Nojima Fault of the 1995 Kobe earthquake. In: Ito H et al (eds) Proceedings of the international workshop on the Nojima fault core and borehole analysis: U S Geol Surv Open-file Rep 00-129. US Geological Survey, Washington, pp 147–152

Lockner DA (1995) Rock failure. In: Ahrens TJ (ed) Rock physics and phase relations: a handbook of physical constants. American Geophysical Union, Washington, pp 127–147

Løseth H, Wensaas L, Arntsen B, Hovland M (2003) Gas and fluid injection triggering shallow mud mobilization in the Hordaland Group, North Sea. Geol Soc Lond Spec Pub 216. Geological Society of London, London, pp 139–157

Lydon JW, Paaki JJ, Anderson HE, Reardon NC (2000) An overview of the geology and geochemistry of the Sullivan deposit. Geol Assoc Can Min Dep Div Spec Pub 1:505–522

McKibben MA, Andrews JP Jr, Williams AE (1988) Active ore formation at a brine interface in metamorphosed deltaic lacustrine sediments: the Salton Sea geothermal system, California. Econ Geol 83:511–523

Marone C, Scholz CH (1988) The depth of seismic faulting and the upper transition from stable to unstable slip regimes. Geophys Res Lett 15:621–624

Mernagh TP, Wyborn LAI, Jagodzinski EA (1998) Unconformity-related U±Au±platinum-group-element deposits. Aust Geol Surv Organ J Aust Geol Geophys 17:197–205

Micarelli L, Benedicto A, Wibberley CAJ (2006) Structural evolution and permeability of normal fault zones in highly porous carbonate rocks. J Struct Geol 28:1214–1227

Moore JC, Saffer D (2001) Updip limit of the seismogenic zone beneath the accretionary prism of southwest Japan: an effect of diagenetic to low-grade metamorphic processes and increasing effective stress. Geology 29:183–186

Myers R, Aydin A (2004) The evolution of faults formed by shearing across joint zones in sandstone. J Struct Geol 26:947–966

Oliver NHS, McLellan JG, Hobbs BE, Cleverley JS, Ord A, Feltrin L (2006) Numerical models of extensional deformation, heat transfer, and fluid flow across basement-cover interfaces during basin-related mineralization. Econ Geol 101:1–31

Pagel M, Poty B, Sheppard SMF (1980) Contributions to some Saskatchewan uranium deposits mainly from fluid inclusion and isotopic data. In: Ferguson S, Goleby A (eds) Uranium in the Pine Creek Geosyncline. International Atomic Energy Authority, Vienna, pp 639–665

Paterson MS, Wong TF (2005) Experimental rock deformation—the brittle field. Springer, New York

Perkins WG, Bell TH (1998) Stratiform replacemen lead-deposits: a comparison between Mount Isa, Hilton, and McArthur River. Econ Geol 93:1190–1212

Rawling GC, Goodwin LB, Wilson JL (2001) Internal architecture, permeability structure, and hydrologic significance of contrasting fault-zone types. Geology 29:43–46

Renard F, Gratier JP, Jamtveit B (2000) Kinetics of crack-sealing, intergranular pressure solution, and compaction around active faults. J Struct Geol 22:1395–1407

Ricard Y, Bercovici D (2003) Two-phase damage theory and crustal rock failure: the theoretical 'void' limit, and the prediction of experimental data. Geophys J Int 155:1057–1064

Roscoe KH, Burland JB (1968) On the generalised stress–strain behavior of 'wet clay'. In: Heyman J, Leckie FA (eds) Engineering plasticity. Cambridge University Press, Cambridge, pp 535–609

Rowland JV, Sibson RH (2004) Structural controls on hydrothermal flow in a segmented rift system, Taupo Volcanic Zone, New Zealand. Geofluids 4:259–283

Rutter EH, Hadizadeh J (1991) On the influence of porosity on the low-temperature brittle–ductile transition in siliciclastic rocks. J Struct Geol 13:609–614

Ruzicka VR (1996) Unconformity-associated uranium. In: Eckstrand OR, Sinclair WD, Thorpe RI (eds) Geology of Canadian mineral deposit types: geology of Canada, 8. Geological Survey of Canada, Ottawa, pp 197–210

Saffer DM, Marone C (2003) Comparison of smectite- and illite-rich gouge frictional properties: application to the updip limit of the seismogenic zone along subduction megathrusts. Earth Planet Sci Lett 215:219–235

Scholz CH (2002) The mechanics of earthquakes and faulting, 2nd edn. Cambridge University Press, Cambridge

Schultz RA, Siddharthan R (2005) A general framework for the occurrence and faulting of deformation bands in porous granular rocks. Tectonophysics 411:1–18

Scott TE, Nielson KC (1991) The effects of porosity on the brittle–ductile transition in sandstones. J Geophys Res 96:405–414

Sheldon HA, Barnicoat AC, Ord A (2006) Numerical modelling of faulting and fluid flow in porous rocks: an approach based on critical state soil mechanics. J Struct Geol 28:1468–1482

Shipton ZK, Cowie PA (2001) Damage zone and slip-surface evolution over μm to km scales in high-porosity Navajo Sandstone, Utah. J Struct Geol 23:1825–1844

Sibson RH (2000) Fluid involvement in normal faulting. J Geodyn 29:469–499

Sibson RH (2001) Seismogenic framework for hydrothermal transport and ore deposition. Rev Econ Geol 14:25–50

Sibson RH, Robert F, Poulsen KH (1988) High-angle reverse faults, fluid-pressure cycling, and mesothermal gold–quartz deposits. Geology 16:551–555

Sigda JM, Goodwin LB, Mozley PS, Wilson JL (1999) Permeability alteration in small-displacement faults in poorly lithified sediments: Rio Grande Rift, Central New Mexico. In: Haneberg WC, Mozley P, Moore JC, Goodwin LB (eds) Faults and subsurface fluid flow in the shallow crust: Geophys Monogr 113. American Geophysical Union, Washington, pp 51–68

Simms MA, Garven G (2004) Thermal convection in faulted extensional sedimentary basins: theoretical results from finite-element modelling. Geofluids 4:109–130

Solomon M, Groves DI (1994) The geology and origin of Australia's mineral deposits. Oxford University Press, Oxford

Southgate PN, Bradshaw BE, Domagala J, Jackson MJ, Idnurm M, Krassay AA, Page RW, Sami TT, Scott DL, Lindsay JF, McConachie BA, Tarlowski C (2000) Chronostratigraphic basin framework for Palaeoproterozoic rocks (1730–1575 Ma) in northern Australia and implications for base metal mineralisation. Aust J Earth Sci 47:461–483

Steiger RP, Leung PK (1991) Critical state shale mechanics. In: Roegiers JC (ed) Rock mechanics as a multidisciplinary science: proceedings—symposium on rock mechanics 32. Balkema, Rotterdam, pp 293–302

Tourigny G, Wilson S, Breton, G, Portella P (2001) Structural controls and emplacement of uranium mineralization at the Sue C deposit, McClean Lake operation, northern Saskatchewan. Saskatchewan Energy and Mines Miscellaneous Report 2001-4.2, Saskatchewan Geological Survey, pp 334–352

Vajdova V, Baud P, Wong TF (2004) Compaction, dilatancy, and failure in porous carbonate rocks. J Geophys Res 109:Article no. B05204

Walderhaug O (1996) Kinetic modeling of quartz cementation and porosity loss in deeply buried sandstone reservoirs. Am Assoc Pet Geol Bull 80:731–745

Wilkinson JJ, Eyre SL, Boyce AJ (2005) Ore-forming processes in Irish-type carbonate-hosted Zn–Pb deposits: evidence from mineralogy, chemistry, and isotopic composition of sulfides at the Lisheen Mine. Econ Geol 100:63–86

Wong TF, Zhu W (1999) Brittle faulting and permeability evolution: hydromechanical measurement, microstructural observation, and network modelling. In: Haneberg WC, Mozley P, Moore JC, Goodwin LB (eds) Faults and subsurface fluid flow in the shallow crust: Geophys Monogr 113. American Geophysical Union, Washington, pp 83–100

Wong TF, David C, Zhu WL (1997) The transition from brittle faulting to cataclastic flow in porous sandstones: mechanical deformation. J Geophys Res 102:3009–3025

Yang J, Large RR, Bull SW (2004) Factors controlling free thermal convection in faults in sedimentary basins: implications for the formation of zinc–lead mineral deposits. Geofluids 4:237–247

Zhang JX, Wong TF, Davis DM (1990) Micromechanics of pressure-induced grain crushing in porous rocks. J Geophys Res 95:341–352

Zhao CB, Hobbs BE, Ord A, Hornby P (2006) Chemical reaction patterns due to fluids mixing and focusing around faults in fluid-saturated porous rocks. J Geochem Explor 89:470–473

Zhu WL, Wong TF (1997) The transition from brittle faulting to cataclastic flow: permeability evolution. J Geophys Res 102:3027–3041